Published in final edited form as:
J Med Chem. 2006 April 6; 49(7): 2268–2275. doi:10.1021/jm050947h.

Design, Synthesis, and Evaluation of Near Infrared Fluorescent Multimeric RGD Peptides for Targeting Tumors

Yunpeng Ye, **Sharon Bloch**, **Baogang Xu**, and **Samuel Achilefu***
Department of Radiology, Washington University, St. Louis, MO 63110

Abstract

Molecular interactions between RGD peptides and integrins are known to mediate many biological and pathological processes. This has led to an increased interest in the development of RGD compounds with high affinity and improved selectivity for integrin receptors. In this study, we synthesized and evaluated a series of multimeric RGD compounds constructed on a dicarboxylic acid-containing near infrared (NIR) fluorescent dye (cypate) for tumor targeting. An array of NIR fluorescent RGD compounds were prepared efficiently, including an RGD monomer (cypate-$(RGD)_2$-NH_2), two RGD dimers (cypate-$(RGD)_2$-NH_2 and cypate-$(RGD\text{-}NH_2)_2$), a trimer (cypate-$(RGD)_3$-NH_2), two tetramers (cypate-$(RGD)_4$-NH_2 and cypate-$[(RGD)_2\text{-}NH_2]_2$), a hexamer (cypate-$[(RGD)_3\text{-}NH_2]_2$), and an octamer (cypate-$[(RGD)_4\text{-}NH_2]_2$). The binding affinity of the multimeric RGD compounds for $\alpha_v\beta_3$ integrin receptor (ABIR) showed a remarkable increase relative to the monomer cypate-RGD-NH_2. Generally, the divalent linear arrays of the multimeric RGD units bound the ABIR with slightly higher affinity than their monovalent analogues. These results suggest that the receptor binding affinity was not only dependent on the number of RGD moieties but also on the spatial alignments of the pendant peptides. Internalization of the compounds by ABIR-positive tumor cells (A549) was monitored by NIR fluorescence microscopy. The data showed that endocytosis of the octameric RGD derivative was significantly higher by comparison to other compounds in this study. *In vivo* noninvasive optical imaging and biodistribution data showed that the compounds were retained in A549 tumor tissue. These results clearly demonstrated that an array of simple RGD tripeptides on a NIR fluorescent dye core can be recognized by ABIR. Optimization of the spatial alignment of the RGD moieties through careful molecular design and library construction could induce multivalent ligand-receptor interactions useful for *in vivo* tumor imaging and tumor-targeted therapy.

Keywords

integrin receptor; molecular recognition; RGD peptide; optical imaging; NIR fluorescent probe; carbocyanine; fluorophore; cypate; multivalent molecular system; synthesis; conjugation; receptor binding; cellular internalization; *in vivo* optical tumor imaging; mice

Introduction

Integrins are a family of heterodimeric transmembrane cell surface receptors that are associated with cell adhesion and metastasis.[1–3] Among them, the $\alpha_V\beta_3$ integrin receptor subtype (ABIR) has received considerable attention because of its expression in a variety of cell types such as endothelial cells,[4–6] platelets,[7–9] osteoclasts,[10–14] melanoma,[15, 16] and smooth muscle cells.[17–19] Many studies have shown that ABIR interacts with some adhesion proteins such

* Corresponding author. Phone: 314-362-8599. Fax: 314-747-5191. E-mail: achilefus@mir.wustl.edu.

as fibronectin, vitronectin, collagen and fibrinogen in the extracellular matrix through a tripeptide arginine-glycine-aspartic acid (RGD) sequence.[20–24] Therefore, RGD peptide ligands that target ABIR are attractive for studying and managing diseases related to their overexpression. To this end, many research groups have focused on developing RGD peptides and analogous compounds for biomedical studies.[25–27] In particular, the roles of integrins in tumor angiogenesis and metastasis have spurred interest in developing integrin-specific RGD peptides and related conjugates for molecular imaging and targeted therapy.[28–36]

Optical imaging is attractive because of its high sensitivity and convenience without the use of ionizing radiation. It has found wide applications in molecular recognitions.[37] For example, Weissleder et al.[38] reported the *in vivo* imaging of tumors with protease-activated near-infrared (NIR) fluorescent probes. Recently, Chen et al.[39] and Wang et al.[40] used a cyanine-labeled cyclic RGD pentapeptide to image brain tumor xenografts in mice by optical method. Burnett et al.[41] reported the synthesis and evaluation of a series of aliphatic carbamate derivatives of the potent non-peptide integrin antagonist for optical imaging of tumors. We have also reported the discovery and development of integrin-targeting cypate-labeled RGD and GRD peptides with high and selective tumor uptake *in vivo* for optical tumor imaging in mice.[42, 43] Such fluorescent molecules not only accelerate the screening of new compounds for lead discovery and optimization at cellular levels, but they are also advantageous in tracking, visualizing, and quantifying target-specific fluorescent probes *in vivo* for distribution and metabolism studies. Particularly, novel NIR fluorescent RGD compounds with improved receptor binding affinity, cellular internalization, and other activities, are needed to improve the sensitivity and specificity of tumor targeting as well as elucidate the structure-activity relationship and related mechanisms of action.

Simultaneous interactions of multiple ligands and multiple receptors (multivalent molecular recognition) are common in biological systems,[44, 45] especially with carbohydrate-mediated biological processes.[46, 47] Interestingly, many native ligands for integrin receptors possess multimeric RGD moieties. For example, fibronectin contains multiple copies of RGD motif for multivalent interactions with integrin receptors in epithelial cells.[45] Both RGD ligand binding to integrins and intracellular activation can induce conformational changes and multimeric clustering of the integrins.[41, 48] Recent reports on the use of multimeric cyclic RGD peptides for ligand endocytosis, imaging angiogenesis, and tumor targeting have demonstrated that multivalency is an efficient strategy for discovering and developing novel RGD compounds with improved integrin recognition in biological systems.[49–51]

Herein, we report the design, synthesis, and evaluation of novel NIR fluorescent multimeric RGD systems based on the simplest RGD motif and cypate. Our results suggest that the number and spatial alignments of pendant RGD moieties on the cypate scaffold can be optimized to harness the advantages of multivalency in biological systems.

Results and Discussion

Chemistry

A host of protein receptors is up-regulated on the cell surfaces of diseased tissues. These provide efficient molecular targets for imaging the stages, progress, and therapeutic response of the diseased tissues, as well as drug delivery based on the molecular recognition between a native or synthetic ligand and the target receptor.[34–36, 52–56] Therefore, the primary goal of this study is to design and develop optimal NIR fluorescent RGD peptides to enhance, visualize and quantify the molecular recognition of RGD peptides by ABIR.

Repeating RGD units—The cyclic RGD pentapeptide, cyclo(RGDfV), binds to integrins with high affinity.[57] Consequently, this peptide has served as a template for the design of

ABIR-avid molecules for diverse biological applications. Most studies previously reported focused on this peptide as a monovalent unit for constructing its multimeric RGD analogues. The importance of the tripeptide RGD motif in the recognition of integrin receptors has inspired us to apply this motif directly as a repeating unit for constructing novel complex multimeric RGD compounds. Compared to the cyclic RGD pentapeptide analogue, the simple RGD peptide sequence allows us to perform efficient peptide assembly and construct a library of diverse molecules on solid support or in solution.

Fluorescent carbocyanine scaffold—Cyanine fluorophores are suitable for *in vitro* and *in vivo* studies because of their high molar extinction coefficient, biocompatibility, and desirable NIR spectral properties between 700–900 nm, where absorption by intrinsic chromophores are weak. This low tissue absorption reduces autofluorescence and allows light to penetrate much deeper in tissue, thereby increasing detection sensitivity of NIR fluorescent dyes. Recently, we improved the synthesis of a dicarboxylic acid-containing carbocyanine fluorophore (cypate) from benzoindole and glutaconaldehyde via pre-acetylation method.[58] Its compatibility with solid phase synthesis enabled us to label diverse peptides, including somatostatin, bombesin, and RGD peptide analogues on solid support.[37, 42] The two carboxylic acid groups of cypate facilitated its use as a fluorescent scaffold to construct diverse complex fluorescent molecular probes such as cypate-based macrocyclic molecules and cypate-cored multivalent carbohydrates.[59, 60] In this study, we focused on cypate as a NIR fluorescent scaffold for preparing multivalent RGD compounds.

Fluorescent multimeric RGD peptides—Although polysaccharides with repeating sequences exist in both linear and dendritic arrays, natural peptides are found primarily in linear arrays. To explore the design, synthesis, evaluation, and structure-activity relationships of multimeric RGD peptides, we initially focused on linear arrays of RGD units on cypate. As shown in Figure 1, a series of NIR fluorescent RGD compounds was designed. The two carboxylic acids of cypate allowed the attachment of one or two RGD peptide chains and each peptide chain may contain one, two, three, or four linear RGD units. One of our goals was to use this molecular design to elucidate the effects of the RGD number and spatial alignment on the ligand molecular recognition by ABIR and *in vivo* tumor targeting.

Synthesis—We used the method described in our previous report to conjugate cypate to resin-bound peptide and obtain the monomeric and dimeric RGD peptide derivatives, simultaneously.[59, 60] We evaluated different coupling reagents and found that the mild coupling condition used in diisopropylcarbodiimide (DIC) procedure typically afforded better yield than the conventional 2-(1-*H* benzotriazole-1-yl)-1,1,1,3-tetramethyluronium hexafluorophosphate (HBTU)/*N*-hydroxybenzotriazole (HOBt)/diisopropylethylamine (DIEA) method on solid supports. As shown in Scheme 1, the protected tripeptide RGD sequence, Arg(Pbf)-Gly-Asp(OBut), was first assembled on Rink amide resin using conventional Fmoc chemistry. Cypate reacted with the resin-bound peptide in the presence of DIC/HOBt, followed by trifluoroacetic acid (TFA) cleavage to afford the desired monomeric (cypate-RGD-NH_2) and dimeric (cypate-$(RGD)_2$-NH_2) fluorescent RGD peptides.

The RGD peptide sequence was further elongated with repeating RGD units on solid support via Fmoc chemistry. Spacers between RGD units were not included in this study to retain the simplicity of the molecular construct and assess the biological effects of the resultant compounds. Different multimeric RGD sequences, including two, three, and four RGD units were obtained. Similarly, conjugation of cypate with these peptides in the presence of DIC/HOBt in DMF, followed by TFA cleavage, afforded the corresponding monovalent linear arrays of a dimeric (cypate-$(RGD)_2$-NH_2), a trimeric (cypate-$(RGD)_3$-NH_2), two tetrameric (cypate-$(RGD)_4$-NH_2 and cypate-$[(RGD)_2$-$NH_2]_2$), a hexameric (cypate-$[(RGD)_3$-$NH_2]_2$), and an octameric (cypate-$[(RGD)_4$-$NH_2]_2$) RGD motifs on cypate. All the compounds were

purified by HPLC and identified by ES-MS. The compounds were fully characterized by the double $[MH_2]^{2+}$, triple $[MH_3]^{3+}$, and other multiply-charged peaks in ES-MS because the presence of many positively charged arginine residues leads to a low abundance of the molecular ion peaks. As the number of RGD moieties increased, the ES-MS spectra became complex with multiple-charged peaks. Particularly, some dehydration peaks accompanied the multiple charged peaks of **9** and **10**. Figure 2 shows that all the compounds exhibited similar UV-vis and emission spectra as cypate in 20% aqueous DMSO solution ($\lambda_{\max}^{abs}$ 784 nm and $\lambda_{\max}^{em}$ 808 nm).

Biological Studies

We evaluated the ABIR binding affinities, cellular internalization, and optical imaging of the new compounds in ABIR-positive cells and tumors in mice.

$\alpha_v\beta_3$ Integrin receptor binding assays—The ABIR binding affinities of all the RGD compounds prepared provided a quantitative measure of the biological effects of the molecular constructs. The IC_{50} of the compounds were determined by using purified ABIR protein and radiolabeled echistatin as tracer. The use of purified protein receptor enhanced reproducibility of the assay. Echistatin is a polypeptide that binds irreversibly with high affinity and specificity to ABIR.[61] Radiolabeling the tyrosine residue with ^{125}I does not affect its ABIR binding affinity. For this reason, ^{125}I-echistatin is used widely as a tracer in ABIR binding assays.[61] Commercially available cyclic RGD pentapeptide, cyclo(RGDfV), was used as a reference standard because it is known to bind ABIR with high affinity.[30] The IC_{50} values obtained are summarized in Table 1.

The competitive binding assays showed that the IC_{50} of the control compound **1** is in the sub-micromolar range relative to the radiolabeled echistatin and provided an index to assess the contribution of multiple RGD repeat units without spacers. Cypate and a non-ABIR-avid cypate-labeled octapeptide (cytate)[62] were used as negative controls. These compounds did not displace the tracer and the gamma counts were similar to those obtained in the absence of a competitor (nonspecific binding). The monomeric **3** and dimeric **4** compounds bound to the receptor, albeit with low affinity relative to other RGD compounds in this study. The low ABIR affinity of these compounds could be attributed to interference of relatively large dye moiety with the ABIR molecular recognition of the small RGD peptide. The ABIR binding affinities of **10** was comparable to the reference standard **1** and the cypate-labeled cyclic RGD peptide **2**. This shows that multiple RGD units without spacers are needed to obtain the high ABIR binding affinity of the conformationally-constrained cyclic peptides **1** and **2**. Overall, the binding affinities increased slightly with an increase in the number of RGD units and followed the general order: **10** > **8** ≈ **6** > **9** > **7** > **5**. This trend splits the multivalent compounds into two classes. The first group (**6**, **8**, and **10**) has high ABIR binding affinities and is derived from a divalent linear arrays of RGD peptides on cypate. The second group with relatively lower affinities (**5**, **7**, and **9**) is derived from monovalent linear arrays of RGD peptides.

These data suggest that the ligand-receptor interaction is somewhat dependent on both the number of repeating RGD units and the structural disposition of the bioactive groups. In this case, it appears that constructing a linear array of RGD on a divalent core enhances ABIR binding affinity of the multimeric RGD motifs. Within the same series, the impact of additional RGD units on the binding affinity varied. While the affinities of the divalent linear arrays of RGD motifs indicate that small increases in the IC_{50} values were obtained with increments of four RGD units (**6** and **10**), affinities of the monovalent linear RGD arrays increased gradually and linearly with the number of RGD units. These findings suggest that starburst multivalent construct could be favorable over linear monovalent repeat RGD units. However, it is entirely possible that different spacing of the RGD repeat units can affect the RGD-ABIR interactions.

Computational modeling could be used to optimize the spatial alignment of the RGD peptide repeat units.

Internalization of multivalent RGD probes in A549 cells—A fluorescence microscope equipped with a 775/50 excitation and 845/55 nm emission filters was used to study the distribution of the compounds in cells. The non-conjugated dye (cypate) was used as a negative control and the fluorescence intensities shown in Figure 3 are relative to that of cypate. Representative cellular images of the compounds are shown in Figure 3. An advantage of imaging in the NIR region is that tissue autofluorescence is low, thereby increasing the sensitivity of the system. All the multimeric RGD compounds internalized into the cells, with **10** giving bright fluorescence by comparison. This observation was expected because **10** contains more RGD units than other compounds. The compounds did not translocate into the cell nucleus, which is important for molecules designed for use as imaging agents. Nuclear internalization of imaging agents is undesirable because of potential mutagenesis of healthy cells. While **6**, **9**, and **10** internalized in the cytoplasm of A549 cells, **5** appears to localize on the cell membrane. However, this did not inhibit the uptake of **5** in tumor bearing mice (see below). To demonstrate the ABIR-mediated uptake, we co-incubated A549 cells with **9** and **1**. Figure 3b shows that compound **1**, which binds to ABIR, inhibited the uptake of **9**, while the fluorescence intensity of the negative control compound (cypate) remained unchanged. The results of the blocking and ABIR binding studies suggest that the simple RGD tripeptide repeat units are recognized by ABIR.

Optical imaging—We evaluated the *in vivo* distribution of three representative compounds, **5**, **6**, and **9** by optical imaging method, as described previously.[62, 63] Compounds **6** and **9** have the same number of RGD units constructed on a monovalent (**9**) and divalent (**6**) cypate core. Nude mice were injected subcutaneously with A549 cells that were allowed to develop into about 5 mm tumors dorsally. The molecular probes were administered retro-orbitally and monitored at 5, 10, and 30 minutes at the initial stages, followed by 1, 4, and 24 h postinjection. Figure 4 shows representative images of **6** and **9** at 24 h postinjection. Background fluorescence of the probes in blood was still high at 4 h postinjection but practically nonexistent after 24 h. The probes preferentially localized in the tumor tissues and the major excretion organs – kidneys and liver.

A limitation of planar fluorescence imaging is in the quantification of the fluorescence intensity map obtained due to light scattering and absorption by tissue. Consequently, the fluorescence intensity of the *in vivo* images obtained is also dependent on the tumor depth from the light source-detector systems. Thus, Figure 4 appears to indicate that the retention of **6** in the tumor is higher than **9**. While this may be correct in terms of the net amount of the probes in the tumor, excision and imaging of tissue parts show that the relative amount of both probes in the tumor are similar. The major differences between the two compounds arise from the rate of tumor uptake and tissue distribution. The tumor is visible with **6** within 4 h postinjection but it was clearly visible with **9** at >12 h postinjection.

We further evaluated the distribution profiles of **5**, **6**, and **9** in mice. Taking the averages of the fluorescence intensity (pixel by pixel) in each tissue, we found that at 24 h postinjection, all three compounds had similar tumor uptake but different distributions in nontarget tissues (Figure 5). The two monovalent linear RGD arrays had higher intensities in the kidneys relative to the divalent analogue **6**. Interestingly, the histogram in Figure 5 also shows that a significant amount of **9** was retained in the animal skin, which further explains the attenuation of the observed fluorescence intensity in the tumor tissue for this compound in living mice (Figure 4). Thus, low skin retention of molecular probes would enhance the contrast obtained by noninvasive optical imaging methods. Overall, the results demonstrate that the simplest RGD peptide sequence can be used to target ABIR-positive tumors. It appears that the ABIR binding

affinities of the probes affect the rate of tumor uptake, with higher affinity probes localizing faster in the tumor than low affinity probes. However, when both low and high affinity binders are retained in the blood for >4 h, the final distribution of the probes in tumor tissue appears to be similar. Thus, compounds possessing high ABIR binding affinities are suitable for rapid delivery of the probes to target tissue, although low binders may be useful for slow deposition of the peptide conjugates to target tissue.

Conclusion

This study describes the first synthesis and evaluation of multimeric arrays of RGD peptides on a near infrared (NIR) fluorescent dye (cypate). It utilized simple RGD units to generate two classes of multimeric RGD motifs on a cypate core. The simplicity of the synthetic strategy makes it feasible to prepare multimeric molecules of higher generation when needed to elucidate the structure-activity relationships. Because of the low absorption of endogenous chromophores in the NIR wavelengths where the dye is photoactive, the fluorescent core also served as the antenna for optical imaging. The *in vitro* data suggest that the molecular design could be used to develop novel compounds with high ABIR binding affinity and cellular internalization. Both the number and spatial alignments of the multivalent RGD units affect the ABIR binding affinity and tumor uptake. In general, a slight increase in ABIR binding affinities with each additional RGD unit was observed. *In vivo*, we observed that compounds with high receptor binding affinities localized faster in the target tumor but after 24 h, the low binding affinity analogues were also retained in the tumor tissue. Thus, the strategy developed in this study provides a template for constructing libraries of diverse biologically relevant molecules for imaging and treating a variety of diseases.

Experimental Section

Solvents and Reagents

HBTU and HOBt were purchased from AnaSpec (San Jose, CA). Trifluoroacetic acid (TFA) and DIEA were purchased from Advanced ChemTech (Louisville, KY). Glutaconaldehyde dianilide monohydrochloride was purchased from Lancaster. Dichloromethane (DCM), *N*, *N*-dimethyformamide (DMF), methanol, and acetonitrile were purchased from Fisher Scientific. Diisopropylcarbodiimide (DIC) and other commercial chemicals were purchased from Sigma-Aldrich. All solvents and chemicals were reagent grade and used without further purification. Cypate was prepared as we reported previously.[58]

Purification and Analysis

HPLC analysis was performed on a Vydac C-18 column (250× 4.6 mm) at a flow rate of 1.0 mL/min. Semi-preparative HPLC was performed on a Vydac C-18 column (25× 2.2 cm) at 9.5 mL/min. HPLC solvents consisted of solvent A (water containing 0.05% TFA) and solvent B (acetonitrile containing 0.05% TFA). The elution protocol for analytical HPLC started with 90% A for 1 min, followed by a linear gradient to 30% A over 20 min, held at 30% A for 5 min, continuing to 10% A over 5 min, and finally returned to 90% A over 2 min. The elution profile was monitored by UV absorbance at 254 nm and 214 nm. Mass spectra were obtained using Shimadzu mass spectrometer (LCMS-2010A) in the positive electrospray mode.

General protocol for solid phase peptide synthesis

All the peptides were assembled manually on Rink amide resin using the conventional Fmoc chemistry in a glass reaction vessel fitted with a sintered glass frit. The coupling reactions were carried out by adding a pre-activated solution of N-α-Fmoc-protected amino acid (3 equiv), HOBt (3 equiv), HBTU (3 equiv), and DIEA (6 equiv) in anhydrous DMF (3 mL/g resin) into the resin (1 equiv) and swirling for 2 h. The progress of the coupling was monitored by Kaiser

test. The Fmoc protecting groups were removed by two 10-min treatments with a solution of 20% piperidine in DMF. The resin was washed with methanol (1 min, 2X) and DMF (1 min, 6X). The resin bound tripeptide, i.e., H-Arg(Pbf)-Gly-Asp(OBut)-NH-Resin (about 1.3 g) was assembled as the monomer from MBHA Rink amide resin (1 g, 0.4 mmol/g) using the general peptide assembly protocol described above. A portion of the resin (~0.1 mmol) was kept for cypate conjugation and the remaining portion was used to assemble the dimeric peptide, i.e., H-[Arg(Pbf)-Gly-Asp(OBut)]$_2$-NH-Resin (~0.1 mmol). Similarly, the trimeric and tetrameric peptides, i.e., H-[Arg(Pbf)-Gly-Asp(OBut)]$_3$-NH-Resin (~0.1 mmol) and H-[Arg(Pbf)-Gly-Asp(OBut)]$_4$-NH-Resin (~0.1 mmol), were obtained by the same procedure.

Cypate-(RGD)$_1$-NH$_2$ (3) and cypate-[(RGD)$_1$-NH$_2$]$_2$ (4)

A mixture of cypate (528 mg, 0.75 mmol), DIC (94.5 mg, 0.75 mmol), HOBt (33.8 mg, 0.25 mmol), and the tripeptide monomer resin, i.e., H-Arg(Pbf)-Gly-Asp(OBut)-NH- Resin (~0.1 mmol) in anhydrous DMF (2 mL) was swirled for 8 h. The resin was filtered, washed with DMF (1 min, 3X), methanol (1 min, 2X), and dried under vacuum. The resin was cleaved with TFA (5 mL, 1.5 h). The TFA filtrate was concentrated and added to cold MBTE (10 mL). The solid precipitate was collected by filtration, washed with petroleum ether, and purified by HPLC to afford the desired compounds:

Compound **3**, 23.5 mg (20% yield), observed m/z for $[MH]^+$, $[2MH_3]^{3+}$, and $[MH_2]^{2+}$ in ES-MS: 951.7, 634.9 (100%), and 476.9.

Compound **4**, 4.8 mg (3% yield), observed m/z for $[MH]^+$, $[MH_2]^{2+}$, and $[MH_3]^{3+}$ in ES-MS: 1281.8, 640.9 (100%), and 427.4.

Cypate-(RGD)$_2$-NH$_2$ (5) and cypate-[(RGD)$_2$-NH$_2$]$_2$ (6)

As described above, the title compounds were prepared similarly from a mixture of cypate (528 mg, 0.75 mmol), DIC (94.5 mg, 0.75 mmol), HOBt (33.8 mg, 0.25 mmol), and the RGD dimer resin, i.e., H-[Arg(Pbf)-Gly-Asp(OBut)]$_2$-NH- Resin (~0.1 mmol) in anhydrous DMF (2 mL). HPLC purification afforded the desired compounds:

Compound **5**, 36 mg (22 % yield) observed m/z for $[MH]^+$, $[MH_2]^{2+}$, and $[MH_3]^{3+}$ in ES-MS: 1280.4, 640.9 (100%), and 427.6.

Compound **6**, 7.5 mg (3% yield), observed m/z for $[MH]^+$, $[MH_2]^{2+}$, $[MH_3]^{3+}$, and $[MH_4]^{4+}$ in ES-MS: 1936.3, 968.8, 646.2 (100%), and 484.9.

Cypate-(RGD)$_3$-NH$_2$ (7) and cypate-[(RGD)$_3$-NH$_2$]$_2$ (8)

As described above, the title compounds were prepared similarly from a mixture of cypate (528 mg, 0.75 mmol), DIC (94.5 mg, 0.75 mmol), HOBt (33.8 mg, 0.25 mmol), and the RGD trimer resin, i.e., H-[Arg(Pbf)-Gly-Asp(OBut)]$_3$-NH- Resin (~0.1 mmol) in anhydrous DMF (2 mL). HPLC purification afforded the desired compounds:

Compound **7**, 41 mg (20% yield), observed m/z for $[MH_2]^{2+}$, $[MH_3]^{3+}$, and $[MH_4]^{4+}$ in ES-MS: 805.0, 537.0 (100%), and 403.1.

Compound **8**, 8.5 mg (3% yield), observed m/z for $[MH_2]^{2+}$, $[MH_3]^{3+}$, and $[MH_4]^{4+}$ in ES-MS: 1297.3, 865.0 (100%), and 649.0.

Cypate-(RGD)$_4$-NH$_2$ (9) and cypate-[(RGD)$_4$-NH$_2$]$_2$ (10)

As described above, the title compounds were prepared similarly from a mixture of cypate (528 mg, 0.75 mmol), DIC (94.5 mg, 0.75 mmol), HOBt (33.8 mg, 0.25 mmol), and the RGD

tetramer resin, i.e., H-[Arg(Pbf)-Gly-Asp(OBut)]$_4$-NH- Resin (~0.1 mmol) in anhydrous DMF (2 mL). HPLC purification afforded the desired compounds:

Compound **9**, 38 mg (15% yield), observed m/z for $[MH_2]^{2+}$, $[MH_2\text{-}H_2O]^{2+}$, and $[MH_3]^{3+}$ in ES-MS: 969.1, 960.3 and 646.5 (100%).

Compound **10**, 8.5 mg (2% yield), observed m/z for $[MH_2]^{2+}$, $[MH_3]^{3+}$, $[MH_3\text{-}H_2O]^{3+}$, $[MH_4]^{4+}$, $[MH_4\text{-}H_2O]^{4+}$, $[MH_5]^{5+}$, $[MH_5\text{-}H_2O]^{5+}$, and $[MH_6\text{-}H_2O]^{6+}$ in ES-MS: 1624.7, 1083.7, 1078.5, 812.8, 808.4, 650.5 (100%), 646.0, and 539.4.

UV-Vis and Emission Analysis

Absorbance spectra were measured on a Beckman Coulter DU 640 UV-Visible spectrophotometer. Fluorescence spectra were recorded on a Fluorolog-3 fluorometer (JOBIN YVON/HORIBA, Edison, New Jersey). Stock solutions (1.0 mM) of the dye and its conjugates were prepared by dissolving each sample in 80% aqueous DMSO. UV-Vis and fluorescence measurements were carried out by sequentially adding 5.0 μL aliquots of the stock solutions via a micropipette into 3 mL of 20% aqueous DMSO solution in a quartz cuvette.

Receptor Binding Determination

Receptor binding assays were performed by using human integrin αVβ3 purified protein from Chemicon International, Inc. (Temecula, CA). Assays were carried out using the Millipore Duropore membrane 96-well plates and the Millipore MultiScreen system (Bedfore, MA). ^{125}I labeling of echistatin (Amersham Biosciences, Piscataway, NJ) was carried out in a mixture of 0.25% BSA, 5.0% lactose, 0.21% citric acid and aprotinin (0.9 TIU/ml). The specific activity of radiolabeled peptide was ~2000 Ci/mmol. Radiochemical purity (90%) was determined by reverse phase HPLC. The 96-well membrane plate was blocked with 0.1% polyethylenimine blocking solution overnight at 4 °C. ^{125}I-echistatin (50 nmol/L) was added to the binding buffer (50 mM Tris-HCl, pH 7.4, 100 mM NaCl, 2 mM $CaCl_2$, 1 mM $MgCl_2$, 1 mM $MnCl_2$, 1 % BSA) containing integrin ABIR protein (50 ng per well in 96-well membrane plate) and ligands in a total volume of 200 μL per well. The concentration range of ligand was between 0.01 μM and 100 μM. The mixtures were incubated for 2 h at room temperature, filtered by centrifugation at 1500 g and washed three times with 0.20 mL of ice-cold binding buffer. The filters containing radioactivity bound ABIR were removed using a punch apparatus and counted using a Packard Cobra II Auto-gamma counter (Meriden, CT). Nonspecific binding of ^{125}I-echistatin was determined to be 5 to 10% of the total binding. The 50% inhibitory concentrations (IC_{50}) were calculated by nonlinear regression analysis by use of the GraphPad Prism 4 computer fitting program (GraphPad Software, Inc., San Diego, CA). Three independent binding assays were performed in triplicates per sample.

Cell Culture

The human non-small cell carcinoma cell line, A549, is widely used to study the role of integrins in normal and pathophysiological processes.[64–72] The A549 cells were purchased from ATCC and grown in 75 cm tissue culture flasks or on Lab-Tek chambered slides in Ham's F12K medium with 2 mM L-glutamine supplemented with 1.5 g/L sodium bicarbonate, 10% fetal calf serum, 100 units/mL Penicillin and 100 units/mL Streptomycin.

Internalization studies

Cells were grown to confluence on LabTek microscope slides. After washing with PBS, the cells were incubated with 1 μM of the target compounds for 1 h. The medium was removed and the cells washed with PBS. The slides were mounted with anti-fading mounting medium.

Cells were visualized with an Olympus microscope system (FV 1000) using 755 excitation and 845 nm emission filters.

Optical Imaging

All *in vivo* studies were performed in compliance with the Washington University Animal Study Committee's requirements for the care and use of laboratory animals in research. Nude mice were anesthetized with xylazine/ketamine cocktail via intraperitoneal injection and placed in a supine position. The nude mice (18–22 g) were injected subcutaneously with A549 cells (1×10^6) in the lower back of the mice. Tumor masses were palpable at 5–7 days post implant, which reached 5 mm in 10–15 days. Prior to injection of the probe, the mice were anesthetized as described above. A 29-gauge was used to inject the probes into the mouse retro-orbitally.

Optical imaging was performed on living mice as described previously using two excitation laser diodes of nominal wavelength 780 nm and nominal power of 50 mW, and a Photometrics CCD camera (16 bit, 1024 × 1024 pixel, back illuminated, thermoelectric Peltier cooled with forced air) equipped with an 830 nm interference filter. The samples were dissolved in 20% aqueous DMSO and animals were injected with doses of 0.3 μmol/kg body weight retro-orbitally. Injected volumes were 100 μL for each mouse. Data analysis consisted of subtracting (pixel by pixel) the pre-injection image from the post injection images, and displaying the false color results. Integration of the relative fluorescence intensities of tumor vs. surrounding tissues indicated the extent of selective uptake of the contrast agent. Noninvasive images of the mice were normalized by comparing the fluorescence intensity of the tumor tissue relative to the contralateral muscle of the animal to minimize the effects of differences in the skin uptake of different probes. At the completion of the study, the mice were euthanized and some tissues were excised and rinsed with water. The tissues were placed under the CCD camera and the fluorescence emission from each organ was measured after excitation with the 780 nm laser sources. A statistical program in the WinView package was used to estimate the mean fluorescence intensity per organ part.

Acknowledgements

This study was supported by research grants from the National Science Foundation (BES 0119489) and the National Institutes of Health (R01 CA109754, R33 CA100972, and R24 CA83060).

References

1. Tsuji T. Physiological and pathological roles of alpha3beta1 integrin. J Membr Biol 2004;200:115–132. [PubMed: 15625821]
2. Gille J, Swerlick RA. Integrins: Role in cell adhesion and communication. Ann N Y Acad Sci 1996;797:93–106. [PubMed: 8993354]
3. Byzova TV, Kim W, Midura RJ, Plow EF. Activation of integrin alpha(v)beta(3) regulates cell adhesion and migration to bone sialoprotein. Exp Cell Res 2000;254:299–308. [PubMed: 10640428]
4. Taverna D, Crowley D, Connolly M, Bronson RT, Hynes RO. A direct test of potential roles for beta3 and beta5 integrins in growth and metastasis of murine mammary carcinomas. Cancer Res 2005;65:10324–10329. [PubMed: 16288021]
5. Carreiras F, Thiebot B, Leroy-Dudal J, Maubant S, Breton MF, Darbeida H. Involvement of alpha v beta 3 integrin and disruption of endothelial fibronectin network during the adhesion of the human ovarian adenocarcinoma cell line igrov1 on the human umbilical vein cell extracellular matrix. Int J Cancer 2002;99:800–808. [PubMed: 12115480]
6. Pedchenko V, Zent R, Hudson BG. Alpha(v)beta3 and alpha(v)beta5 integrins bind both the proximal rgd site and non-rgd motifs within noncollagenous (nc1) domain of the alpha3 chain of type iv collagen:

Implication for the mechanism of endothelia cell adhesion. J Biol Chem 2004;279:2772–2780. [PubMed: 14610079]

7. Pidgeon GP, Tang K, Cai YL, Piasentin E, Honn KV. Overexpression of platelet-type 12-lipoxygenase promotes tumor cell survival by enhancing alpha(v)beta(3) and alpha(v)beta(5) integrin expression. Cancer Res 2003;63:4258–4267. [PubMed: 12874035]
8. Mousa SA, Forsythe M, Bozarth J, Jin F, Confalone PN. Human platelet alphaiibeta3 integrin binding affinity and specificity of sj874: Antiplatelet efficacy versus aspirin. Coron Artery Dis 2000;11:563–570. [PubMed: 11023245]
9. Watson SP, Auger JM, McCarty OJT, Pearce AC. Gpvi and integrin alpha ii beta 3 signaling in platelets. J Thromb Haemost 2005;3:1752–1762. [PubMed: 16102042]
10. Nakamura I, Jimi E. Role of alpha v beta 3 integrins in osteoclast function. Recent Res Dev Immunol 2004;6:79–94.
11. Inoue M, Namba N, Chappel J, Teitelbaum SL, Ross FP. Granulocyte macrophage-colony stimulating factor reciprocally regulates alphav-associated integrins on murine osteoclast precursors. Mol Endocrinol 1998;12:1955–1962. [PubMed: 9849968]
12. Sago K, Teitelbaum SL, Venstrom K, Reichardt LF, Ross FP. The integrin alphavbeta5 is expressed on avian osteoclast precursors and regulated by retinoic acid. J Bone Miner Res 1999;14:32–38. [PubMed: 9893063]
13. Lane NE, Yao W, Nakamura MC, Humphrey MB, Kimmel D, Huang X, Sheppard D, Ross FP, Teitelbaum SL. Mice lacking the integrin beta5 subunit have accelerated osteoclast maturation and increased activity in the estrogen-deficient state. J Bone Miner Res 2005;20:58–66. [PubMed: 15619670]
14. McHugh KP, Hodivala-Dilke K, Zheng MH, Namba N, Lam J, Novack D, Feng X, Ross FP, Hynes RO, Teitelbaum SL. Mice lacking beta3 integrins are osteosclerotic because of dysfunctional osteoclasts. J Clin Invest 2000;105:433–440. [PubMed: 10683372]
15. Li X, Chen B, Blystone SD, McHugh KP, Ross FP, Ramos DM. Differential expression of alphav integrins in k1735 melanoma cells. Invasion Metastasis 1998;18:1–14. [PubMed: 10207246]
16. Kuphal S, Bauer R, Bosserhoff AK. Integrin signaling in malignant melanoma. Cancer Metastasis Rev 2005;24:195–222. [PubMed: 15986132]
17. Bilato C, Curto KA, Monticone RE, Pauly RR, White AJ, Crow MT. The inhibition of vascular smooth muscle cell migration by peptide and antibody antagonists of the alphavbeta3 integrin complex is reversed by activated calcium/calmodulin- dependent protein kinase ii. J Clin Invest 1997;100:693–704. [PubMed: 9239418]
18. Kintscher U, Lyon C, Wakino S, Bruemmer D, Xu F, Goetze S, Graf K, Moustakas A, Staels B, Fleck E, Hsueh WA, Law RE. Ppar alpha inhibits tgf-beta-induced beta(5) integrin transcription in vascular smooth muscle cells by interacting with smad4. Circ Res 2002;91:E35–E44. [PubMed: 12456495]
19. Lygoe KA, Norman JT, Marshall JF, Lewis MP. Alphav integrins play an important role in myofibroblast differentiation. Wound Repair Regen 2004;12:461–470. [PubMed: 15260812]
20. Pierschbacher MD, Ruoslahti E. Cell attachment activity of fibronectin can be duplicated by small synthetic fragments of the molecule. Nature 1984;309:30–33. [PubMed: 6325925]
21. Pierschbacher MD, Hayman EG, Ruoslahti E. The cell attachment determinant in fibronectin. J Cell Biochem 1985;28:115–126. [PubMed: 3908463]
22. Ruoslahti E, Pierschbacher MD. Arg-gly-asp: A versatile cell recognition signal. Cell 1986;44:517–518. [PubMed: 2418980]
23. Ruoslahti E. The rgd story: A personal account. Matrix Biol 2003;22:459–465. [PubMed: 14667838]
24. Busk M, Pytela R, Sheppard D. Characterization of the integrin alpha v beta 6 as a fibronectin-binding protein. J Biol Chem 1992;267:5790–5796. [PubMed: 1532572]
25. Paik JY, Ko BH, Yearn SC, Choi Y, Lee KH, Kim BT. Pma-enhanced neutrophil [18f]fdg uptake is independent of integrin occupancy but requires pi3k activity. Nucl Med Biol 2005;32:561–566. [PubMed: 16026702]
26. Bergh JJ, Lin HY, Lansing L, Davis FB, Davis PJ, Mohamed SN, Mousa S. Integrin alpha v beta 3 contains a cell surface receptor site for thyroid hormone that is linked to activation of mitogen-activated protein kinase and induction of angiogenesis. Endocrinology 2005;146:2864–2871. [PubMed: 15802494]

27. Fondevila C, Shen XD, Moore C, Busuttil RW, Coito AJ. Cyclic rgd peptides with high affinity for alpha 5 beta 1 integrin protect genetically fat zucker rat livers from cold ischemia/reperfusion injury. Transplant Proc 2005;37:1679–1681. [PubMed: 15919428]
28. Haubner R, Wester HJ, Burkhart F, Senekowitsch-Schmidtke R, Weber W, Goodman SL, Kessler H, Schwaiger M. Glycosylated rgd-containing peptides, tracer for tumor targeting and angiogenesis imaging with improved biokinetics. J Nucl Med 2001;42:326–336. [PubMed: 11216533]
29. Aumailley M, Gurrath M, Muller G, Calvete J, Timpl R, Kessler H. Arg-gly-asp constrained within cyclic pentapeptides. Strong and selective inhibitors of cell adhesion to vitronectin and laminin fragment p1. FEBS Lett 1991;291:50–54. [PubMed: 1718779]
30. Dechantsreiter MA, Planker E, Matha B, Lohof E, Holzemann G, Jonczyk A, Goodman SL, Kessler H. N-methylated cyclic rgd peptides as highly active and selective alpha(v)beta(3) integrin antagonists. J Med Chem 1999;42:3033–3040. [PubMed: 10447947]
31. Haubner R, Kuhnast B, Mang C, Weber WA, Kessler H, Wester HJ, Schwaiger M. F-18 galacto-rgd: Synthesis, radiolabeling, metabolic stability, and radiation dose estimates. Bioconjug Chem 2004;15:61–69. [PubMed: 14733584]
32. Nisato RE, Tille JC, Jonczyk A, Goodman SL, Pepper MS. Alphav beta 3 and alphav beta 5 integrin antagonists inhibit angiogenesis in vitro. Angiogenesis 2003;6:105–119. [PubMed: 14739617]
33. Enns A, Korb T, Schluter K, Gassmann P, Spiegel HU, Senninger N, Mitjans F, Haier J. Alphavbeta5-integrins mediate early steps of metastasis formation. Eur J Cancer 2005;41:1065–1072. [PubMed: 15862757]
34. Kessler T, Bieker R, Padro T, Schwoppe C, Persigehl T, Bremer C, Kreuter M, Berdel WE, Mesters RM. Inhibition of tumor growth by rgd peptide-directed delivery of truncated tissue factor to the tumor vasculature. Clin Cancer Res 2005;11:6317–6324. [PubMed: 16144936]
35. Mitra A, Mulholland J, Nan A, McNeill E, Ghandehari H, Line BR. Targeting tumor angiogenic vasculature using polymer-rgd conjugates. J Control Release 2005;102:191–201. [PubMed: 15653145]
36. Tucker GC. Alpha v integrin inhibitors and cancer therapy. Curr Opin Investig Drugs 2003;4:722–731.
37. Achilefu S. Lighting up tumors with receptor-specific optical molecular probes. Technol Cancer Res Treat 2004;3:393–409. [PubMed: 15270591]
38. Weissleder R, Tung CH, Mahmood U, Bogdanov A. In vivo imaging of tumors with protease-activated near-infrared fluorescent probes. Nat Biotechnol 1999;17:375–378. [PubMed: 10207887]
39. Chen X, Conti PS, Moats RA. In vivo near-infrared fluorescence imaging of integrin alpha v beta 3 in brain tumor xenografts. Cancer Res 2004;64:8009–8014. [PubMed: 15520209]
40. Wang W, Ke S, Wu Q, Charnsangavej C, Gelovani JG, Abbruzzese JL, Li C, Gurfinkel M, Sevick-Muraca EM. Near-infrared optical imaging of integrin alpha v beta 3 in human tumor xenografts. Molecular Imaging 2004;3:343–351. [PubMed: 15802051]
41. Burnett CA, Xie J, Quijano J, Hunter F, Bur M, Li KCP, Danthi SN, Shen Z. Synthesis, in vitro, and in vivo characterization of an integrin alpha v beta 3-targeted molecular probe for optical imaging of tumor. Bioorg Med Chem 2005;13:3763–3771. [PubMed: 15863003]
42. Achilefu S, Bloch S, Markiewicz MA, Zhong TX, Ye YP, Dorshow RB, Chance B, Liang KX. Synergistic effects of light-emitting probes and peptides for targeting and monitoring integrin expression. Proc Natl Acad Sci U S A 2005;102:7976–7981. [PubMed: 15911748]
43. Bloch S, Liang K, Dorshow RB, Ye Y, Achilefu S. Targeting the expression of integrin receptors in tumors. Proc SPIE 2004;5329:222–228.
44. Sharma SD, Jiang JW, Hadley ME, Bentley DL, Hruby VJ. Melanotropic peptide-conjugated beads for microscopic visualization and characterization of melanoma melanotropin receptors. Proc Natl Acad Sci U S A 1996;93:13715–13720. [PubMed: 8943000]
45. Mammen M, Choi SK, Whitesides GM. Polyvalent interactions in biological systems: Implications for design and use of multivalent ligands and inhibitors. Angew Chem-Int Edit 1998;37:2755–2794.
46. Roy R. A decade of glycodendrimer chemistry. Trends Glycosci Glycotechnol 2003;15:291–310.
47. Sacchettini JC, Baum LG, Brewer CF. Multivalent protein-carbohydrate interactions. A new paradigm for supermolecular assembly and signal transduction. Biochemistry 2001;40:3009–3015. [PubMed: 11258914]

48. Burridge K, Chrzanowska-Wodnicka M. Focal adhesions, contractility, and signaling. Annu Rev Cell Dev Biol 1996;12:463–518. [PubMed: 8970735]
49. Thumshirn G, Hersel U, Kessler H, Goodman SL. Multimeric cyclic rgd peptides as potential tools for tumor targeting: Solid-phase peptide synthesis and chemoselective oxime ligation. Chem-Eur J 2003;9:2717–2725.
50. Boturyn D, Garanger E, Dumy P, Coll JL, Favrot MC. Template assembled cyclopeptides as multimeric system for integrin targeting and endocytosis. J Am Chem Soc 2004;126:5730–5739. [PubMed: 15125666]
51. Dirksen A, Langereis S, De Waal BFM, Van Genderen MHP, Meijer EW, Hackeng TM. A supramolecular approach to multivalent target-specific mri contrast agents for angiogenesis. Chem Commun 2005:2811–2813.
52. Winnard P Jr, Raman V. Real time non-invasive imaging of receptor-ligand interactions in vivo. J Cell Biochem 2003;90:454–463. [PubMed: 14523979]
53. Leamon CP, Reddy JA. Folate-targeted chemotherapy. Adv Drug Deliv Rev 2004;56:1127–1141. [PubMed: 15094211]
54. Ke CY, Mathias CJ, Green MA. Folate-receptor-targeted radionuclide imaging agents. Adv Drug Deliv Rev 2004;56:1143–1160. [PubMed: 15094212]
55. Cheng Z, Wu Y, Xiong Z, Gambhir SS, Chen X. Near-infrared fluorescent rgd peptides for optical imaging of integrin alphavbeta3 expression in living mice. Bioconjug Chem 2005;16:1433–1441. [PubMed: 16287239]
56. Tung CH, Lin YH, Moon WK, Weissleder R. A receptor-targeted near-infrared fluorescence probe for in vivo tumor imaging. Chembiochem 2002;3:784–786. [PubMed: 12203978]
57. Gottschalk KE, Kessler H. The structures of integrins and integrin-ligand complexes: Implications for drug design and signal transduction. Angew Chem-Int Edit 2002;41:3767–3774.
58. Ye Y, Li WP, Anderson CJ, Kao J, Nikiforovich GV, Achilefu S. Synthesis and characterization of a macrocyclic near-infrared optical scaffold. J Am Chem Soc 2003;125:7766–7767. [PubMed: 12822971]
59. Ye YP, Bloch S, Achilefu S. Polyvalent carbocyanine molecular beacons for molecular recognitions. J Am Chem Soc 2004;126:7740–7741. [PubMed: 15212497]
60. Ye Y, Bloch S, Kao J, Achilefu S. Multivalent carbocyanine molecular probes: Synthesis and applications. Bioconjug Chem 2005;16:51–61. [PubMed: 15656575]
61. Kumar CC, Nie HM, Rogers CP, Malkowski M, Maxwell E, Catino JJ, Armstrong L. Biochemical characterization of the binding of echistatin to integrin alpha(v)beta(3) receptor. J Pharmacol Exp Ther 1997;283:843–853. [PubMed: 9353406]
62. Achilefu S, Dorshow RB, Bugaj JE, Rajagopalan R. Novel receptor-targeted fluorescent contrast agents for in vivo tumor imaging. Invest Radiol 2000;35:479–485. [PubMed: 10946975]
63. Bugaj JE, Achilefu S, Dorshow RB, Rajagopalan R. Novel fluorescent contrast agents for optical imaging of in vivo tumors based on a receptor-targeted dye-peptide conjugate platform. J Biomed Opt 2001;6:122–133. [PubMed: 11375721]
64. Cordes N, Beinke C, Plasswilm L, van Beuningen D. Irradiation and various cytotoxic drugs enhance tyrosine phosphorylation and beta(1)-integrin clustering in human a549 lung cancer cells in a substratum-dependent manner in vitro. Strahlenther Onkol 2004;180:157–164. [PubMed: 14991204]
65. Oyama T, Sykes KF, Samli KN, Minna JD, Johnston SA, Brown KC. Isolation of lung tumor specific peptides from a random peptide library: Generation of diagnostic and cell-targeting reagents. Cancer Lett 2003;202:219–230. [PubMed: 14643452]
66. Lubin FD, Segal M, McGee DW. Regulation of epithelial cell cytokine responses by the alpha 3 beta 1 integrin. Immunology 2003;108:204–210. [PubMed: 12562329]
67. Davison E, Kirby I, Whitehouse J, Hart I, Marshall JF, Santis G. Adenovirus type 5 uptake by lung adenocarcinoma cells in culture correlates with ad(5) fibre binding is mediated by alpha(v)beta(1) integrin and can be modulated by changes in beta(1) integrin function. J Gene Med 2001;3:550–559. [PubMed: 11778901]
68. Triantafilou K, Triantafilou M, Takada Y, Fernandez N. Human parechovirus 1 utilizes integrins alpha v beta 3 and alpha v beta 1 as receptors. J Virol 2000;74:5856–5862. [PubMed: 10846065]

69. Allen CM, Sharman WM, La Madeleine C, Weber JM, Langlois R, Ouellet R, van Lier JE. Photodynamic therapy: Tumor targeting with adenoviral proteins. Photochem Photobiol 1999;70:512–523. [PubMed: 10546549]

70. Pottratz ST, Weir AL. Gamma-interferon inhibits pneumocystis carinii attachment to lung cells by decreasing expression of lung cell-surface integrins. Eur J Clin Invest 1997;27:17–22. [PubMed: 9041372]

71. Reilly PL, Woska JR, Jeanfavre DD, McNally E, Rothlein R, Bormann BJ. The native structure of intercellular-adhesion molecule-1 (icam-1) is a dimer - correlation with binding to lfa-1. J Immunol 1995;155:529–532. [PubMed: 7608533]

72. Bai M, Campisi L, Freimuth P. Vitronectin receptor antibodies inhibit infection of hela and a549 cells by adenovirus-type-12 but not by adenovirus type-2. J Virol 1994;68:5925–5932. [PubMed: 7520097]

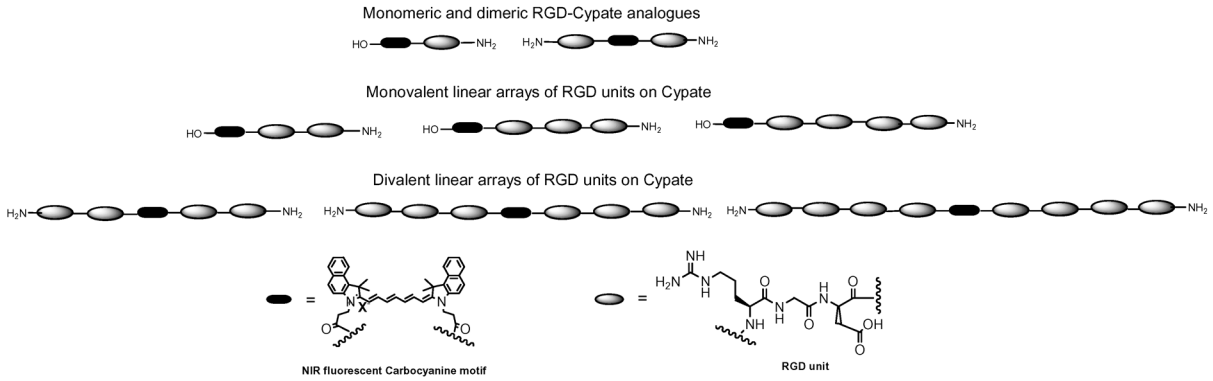

Figure 1.
Design of novel NIR fluorescent multimeric RGD peptides based on a dicarboxylic acid-containing carbocyanine (cypate).

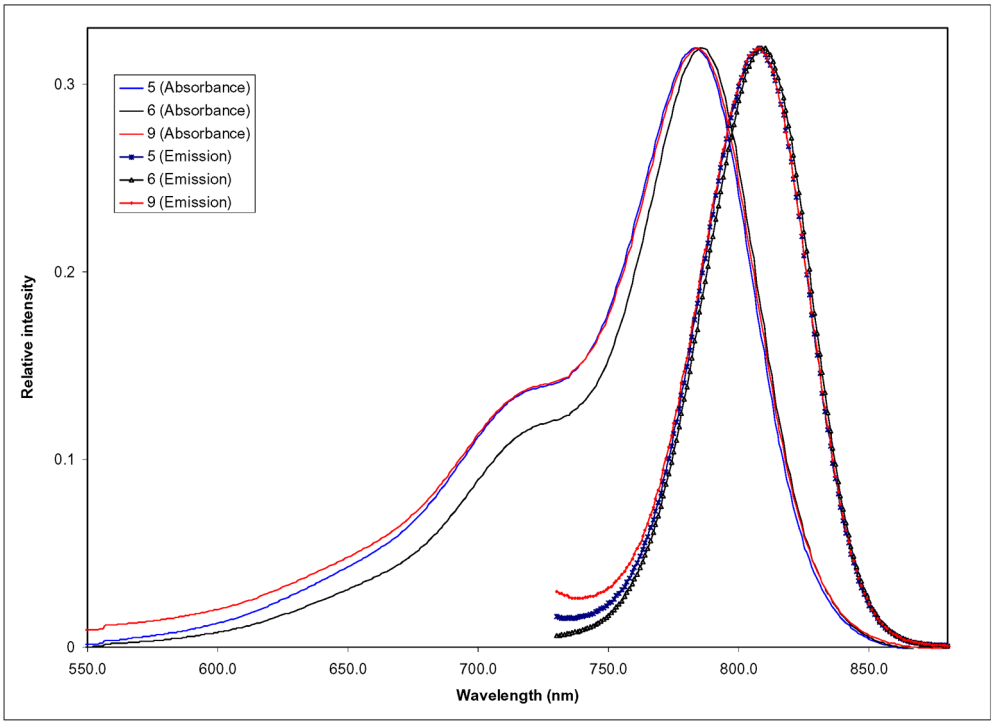

Figure 2.
Normalized UV-vis and emission spectra of representative multimeric RGD compounds in 20% aq. DMSO solution.

Figure 3a

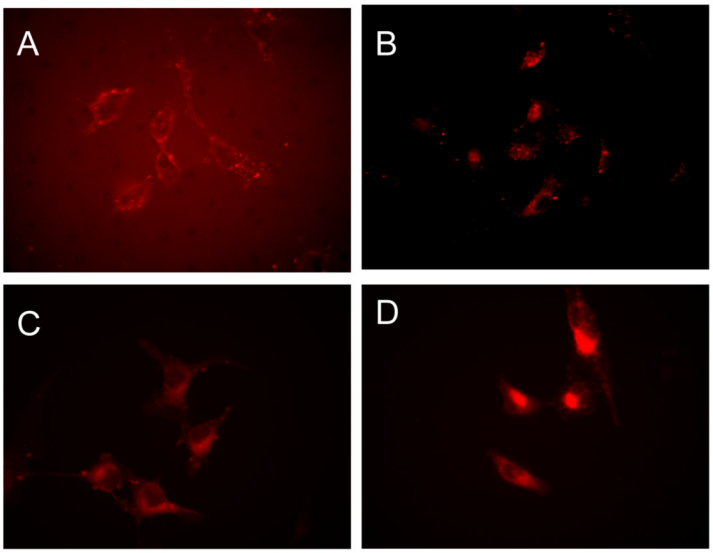

Figure 3b

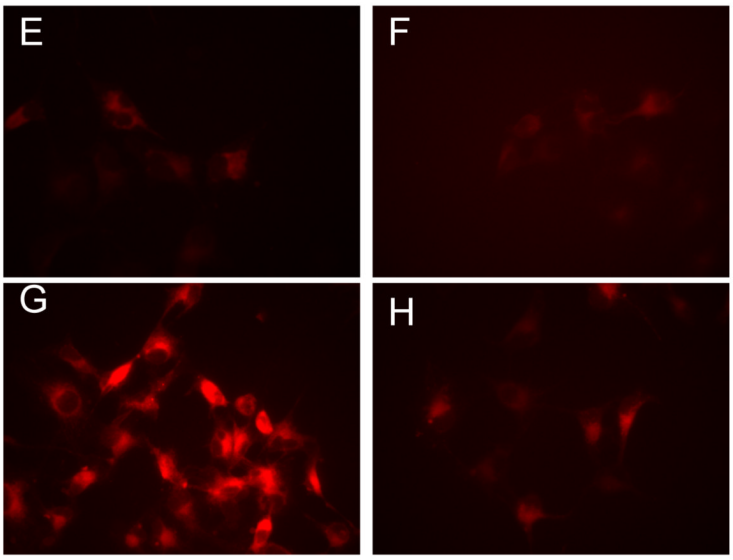

Figure 3.

Figure 3a. A549 cells treated with 1 μM of compounds (A) **5**, (B) **6**, (C) **9**, and (D) **10** for 1 h at 37 °C. Arbitrary intensity scale is 300 to 650 for **5**, **6**, and **9**. The intensity scale for 10 is 300 (black) to 1500 (red) because of the exceptionally high fluorescence intensity relative to other compounds in the figure.

Figure 3b. A549 cells incubated with 1μM of cypate (E and F) and **9** (G and H) for 45 min 37 °C, without (E and G) or with (F and H) 1 h pretreatment with 100 μM of cyclo(RGDfV) that binds ABIR. The intensity scale for 1128 ms exposure is 200 (black) to 600 (red).

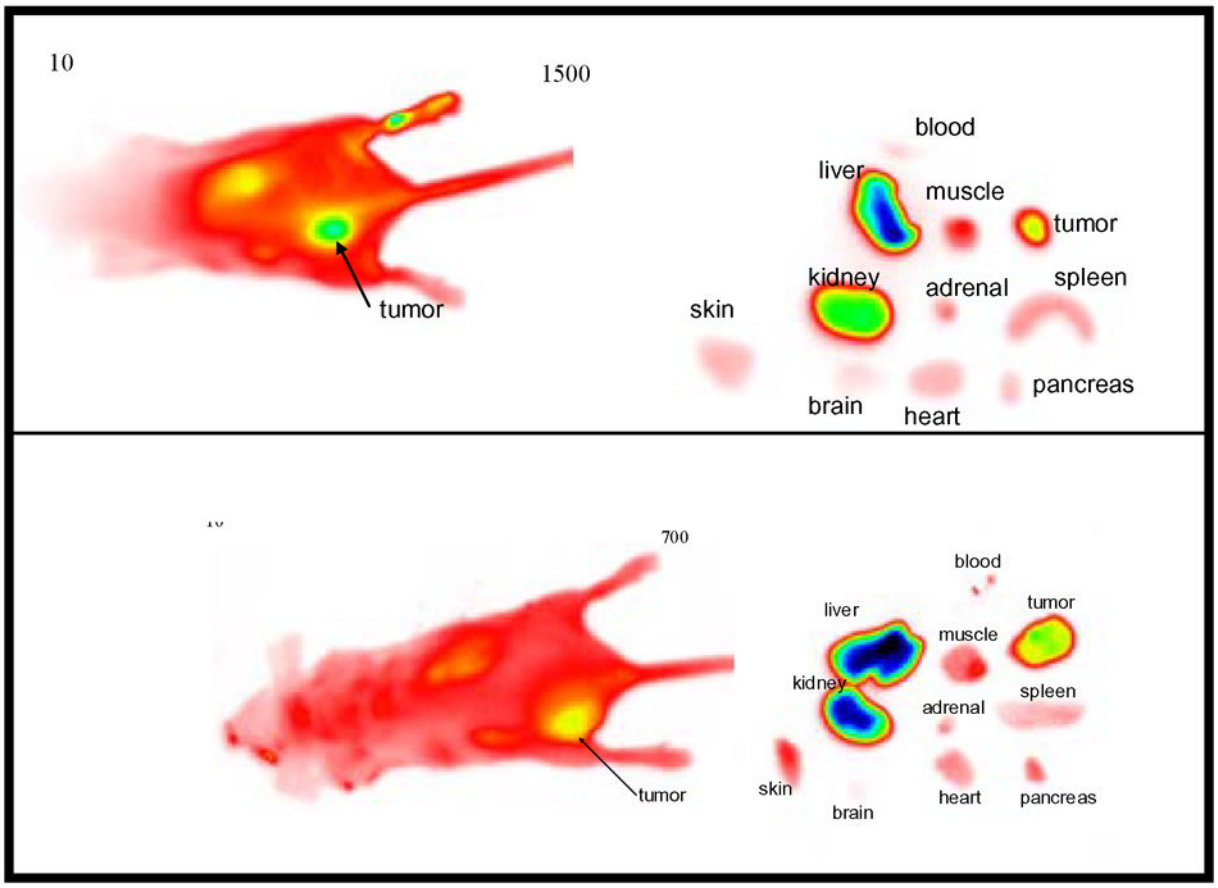

Figure 4.
Whole-body optical imaging of **6** (top) and **9** (bottom) at 24 h postinjection of the probes. False color image: red, low; yellow, medium; green, medium-high; blue, high

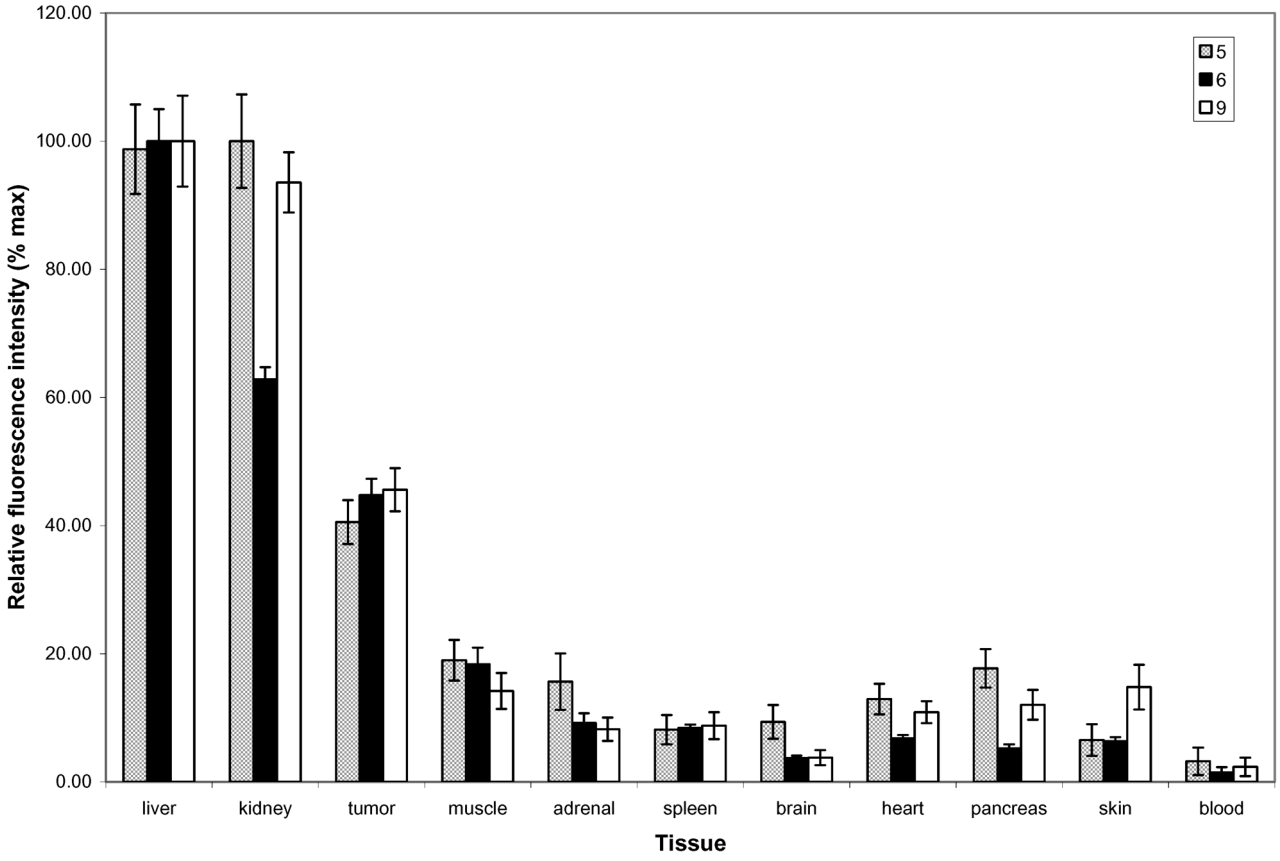

Figure 5.
Biodistribution of compounds **5**, **6**, and **9** in A549 tumor bearing nude mice

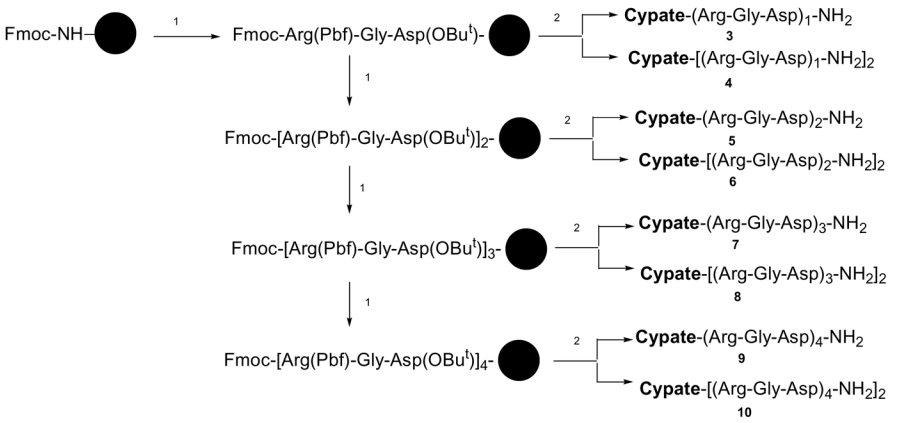

Reagents and condition: 1. Conventional Fmoc chemistry, i.e., a) Piperidine/DMF (20%); b) Fmoc-AA/HOBT/HBTU/DIEA/DMF; 2. a) Piperidine/DMF (20%); b) Cypate/DIC/HOBT/rt/8h; c) TFA.

Scheme 1.

Synthesis of linearly arrayed multimeric RGD-cypate conjugates on a solid support

Table 1

The IC_{50} values of the RGD compounds prepared using purified ABIR proteins and ^{125}I-echistatin as radiotracer

#	Structure	IC_{50} (M)
1	Cyclo(RGDfV) - Control	$2.87 \pm 0.97 \times 10^{-8}$
2	Cyclo[RGDfK(cypate)]	$6.39 \pm 2.28 \times 10^{-8}$
3	Cypate-$[(RGD)_1$-$NH_2)]_1$	Not applicable*
4	Cypate-$[(RGD)_1$-$NH_2)]_2$	Not applicable
5	Cypate-$[(RGD)_2$-$NH_2]_1$	$7.3 \pm 1.38 \times 10^{-7}$
6	Cypate-$[(RGD)_2$-$NH_2]_2$	$1.04 \pm 0.05 \times 10^{-7}$
7	Cypate-$[(RGD)_3$-$NH_2]_1$	$4.81 \pm 0.78 \times 10^{-7}$
8	Cypate-$[(RGD)_3$-$NH_2]_2$	$1.32 \pm 0.27 \times 10^{-7}$
9	Cypate-$[(RGD)_4$-$NH_2]_1$	$2.59 \pm 0.02 \times 10^{-7}$
10	Cypate-$[(RGD)_4$-$NH_2]_2$	$7.96 \pm 2.5 \times 10^{-8}$

*Values of IC_{50} >1 μM were not determined due to limitation of the assay protocol